



Cutaneous Epithelial to Mesenchymal Transition Activator ZEB1 Regulates Wound Angiogenesis and Closure in a Glycemic Status–Dependent Manner

Kanhaiya Singh,^{1,2} Mithun Sinha,^{1,2} Durba Pal,^{2,3} Saba Tabasum,^{1,2} Surya C. Gnyawali,² Dolly Khona,^{1,2} Subendu Sarkar,^{1,2} Sujit K. Mohanty,¹ Fidel Soto-Gonzalez,² Savita Khanna,^{1,2} Sashwati Roy,^{1,2} and Chandan K. Sen^{1,2}

Diabetes 2019;68:2175–2190 | <https://doi.org/10.2337/db19-0202>

Epithelial to mesenchymal transition (EMT) and wound vascularization are two critical interrelated processes that enable cutaneous wound healing. Zinc finger E-box binding homeobox 1 (ZEB1), primarily studied in the context of tumor biology, is a potent EMT activator. ZEB1 is also known to contribute to endothelial cell survival as well as stimulate tumor angiogenesis. The role of ZEB1 in cutaneous wounds was assessed using *Zeb1*^{+/-} mice, as *Zeb1*^{-/-} mice are not viable. Quantitative stable isotope labeling by amino acids in cell culture (SILAC) proteomics was used to elucidate the effect of elevated ZEB1, as noted during hyperglycemia. Under different glycemic conditions, ZEB1 binding to E-cadherin promoter was investigated using chromatin immunoprecipitation. Cutaneous wounding resulted in loss of epithelial marker E-cadherin with concomitant gain of ZEB1. The dominant proteins downregulated after ZEB1 overexpression functionally represented adherens junction pathway. *Zeb1*^{+/-} mice exhibited compromised wound closure complicated by defective EMT and poor wound angiogenesis. Under hyperglycemic conditions, ZEB1 lost its ability to bind E-cadherin promoter. Keratinocyte E-cadherin, thus upregulated, resisted EMT required for wound healing. Diabetic wound healing was improved in *ZEB*^{+/-} as well as in *db/db* mice subjected to ZEB1 knockdown. This work recognizes ZEB1 as a key regulator of cutaneous wound healing that is of particular relevance to diabetic wound complication.

Diabetes complicates cutaneous wound closure, as evident by stalled wound reepithelialization and compromised

angiogenesis (1,2). These rate-limiting events in wound healing require a tight interplay between factors governing epithelial to mesenchymal transition (EMT) and wound vascularization (3,4). A transient process, reminiscent of EMT, is required during the early phase of cutaneous wound healing to restore the epidermal homeostasis. Induced by injury, this process activates and mobilizes stationary keratinocytes in the skin toward the wound bed, enabling reepithelialization (3). Concurrently, sprouting of angiogenic capillaries and their organization in microvascular network are essential to support the elevated metabolic demands of the repairing tissue (5).

Primarily studied in tumor biology, ZEB1 is a potent EMT activator (6–8). In the skin, *Zeb1* is known to be localized to dermal fibroblasts, melanocytes, and Langerhans cells (9–11). In response to injury, *Zeb1* is induced in epithelial cells and macrophages (12,13). Cutaneous ZEB1 is a transcriptional repressor of epithelial genes like E-cadherin (14). Such loss of E-cadherin is known to cause EMT (15,16). Furthermore, ZEB1 stimulates angiogenesis via induction of vascular endothelial growth factor (VEGF)-A (17) and acting as an endothelial cell survival factor (18). It was therefore of interest to test the significance of ZEB1 in cutaneous wound healing. As part of that pursuit, diabetic wounds were studied to test ZEB1 and its potential role in compromised healing. This effort led to a striking observation recognizing that under hyperglycemic conditions, as noted in *db/db* mice, ZEB1 is induced

¹Indiana Center for Regenerative Medicine and Engineering, Indiana University Health Comprehensive Wound Center, Indiana University School of Medicine, Indianapolis, IN

²Comprehensive Wound Center, Center for Regenerative Medicine and Cell Based Therapies, Department of Surgery, The Ohio State University Wexner Medical Center, Columbus, OH

³Center for Biomedical Engineering, Indian Institute of Technology Ropar, Punjab, India

Corresponding author: Chandan K. Sen, cksen@iu.edu

Received 27 February 2019 and accepted 15 August 2019

This article contains Supplementary Data online at <http://diabetes.diabetesjournals.org/lookup/suppl/doi:10.2337/db19-0202/-/DC1>.

© 2019 by the American Diabetes Association. Readers may use this article as long as the work is properly cited, the use is educational and not for profit, and the work is not altered. More information is available at <http://www.diabetesjournals.org/content/license>.

by two orders of magnitude in the skin. Furthermore, under such conditions ZEB1 loses its ability to bind the E-cadherin promoter. Such loss of negative regulation of E-cadherin expression results in elevated E-cadherin, which in turn is known to resist EMT, a process required for wound healing (19,20). Under diabetic conditions, extraordinarily high ZEB1 also compromises wound angiogenesis. Diabetic wound healing is improved in *Zeb*^{+/-} mice, which identifies ZEB1 as a novel therapeutic target.

In this work, we sought to test the hypothesis that low ZEB1 expression compromises cutaneous wound healing because of inadequate transient wound EMT and angiogenesis. Quantitative triple-labeling stable isotope labeling by amino acids in cell culture (SILAC) analysis revealed the ripple effect of ZEB1 overexpression on the epithelial cell proteome. Chromatin immunoprecipitation (ChIP) followed by immunoprecipitation–mass spectrometry identified the differential binding activity of ZEB1 to E-cadherin promoter and other proteins under normoglycemic and hyperglycemic conditions. Of outstanding interest was the observation that hyperglycemic culture of endothelial cells markedly decreased the binding of ZEB1 to the promoter of E-cadherin and other specific inflammatory proteins such as α -enolase (ENO1) and S100A8/A9. Deficiency of ZEB1 rescued diabetic wound angiogenesis. This work recognizes ZEB1 as a critical determinant of wound angiogenesis under physiological and diabetic conditions.

RESEARCH DESIGN AND METHODS

Reagents and Antibodies

Tissue culture materials were procured from Thermo Fisher Scientific (Waltham, MA). ON-TARGETplus Nontargeting siRNA control (cat. no. D-001810-01-05) and *ZEB1* siRNA SMARTpool (L-006564-01-0005) were bought from GE Dharmacon (Lafayette, CO). For in vivo *Zeb1* knockdown studies, siRNA vector against mice *Zeb1* (piLenti-si-Zeb1-GFP) or scrambled siRNA vector (cat. no. LVP015-G) was procured from Applied Biological Materials (Richmond, BC). For ZEB1 overexpression studies, ZEB1 Lentiviral Vector, human (cat. no. LV362464), was purchased from Applied Biological Materials. As controls, we used pLenti-III-Blank Vector without the insert synthesized by Applied Biological Materials (cat. no. LV587). Antibodies against VE-cadherin (ab33168), anti-FSP-1 (ab27957), anti- β -catenin (ab16051), VEGF (ab46154), anti-collagen IV (ab19808), vWF (ab6994), and smooth muscle actin (SMA) (ab5694) were purchased from Abcam (Cambridge, MA). E-cadherin antibody (13-1900) and ChIP-grade anti-ZEB1 antibody (cat. no. PA528221) were purchased from Thermo Fisher Scientific. Rat anti-mouse CD31 (cat. no. 550274) was purchased from BD Pharmingen, San Jose, CA. Anti-human CD31-APC antibody (clone: WM59, cat. no. 303115) was bought from BioLegend (San Diego, CA). F4/80 antibody (cat. no. MCA497) was bought from Bio-Rad (Hercules, CA). Corning Matrigel Matrix (cat. no. 354234) was obtained from Corning Inc.

(Corning, NY), and agarose bead-based SimpleChIP Plus Enzymatic Chromatin IP Kit (9004) was purchased from Cell Signaling Technology (Danvers, MA).

Cell Culture

Human dermal microvascular endothelial cells (HMECs) were maintained in MCDB-131 medium (cat. no. 10372-019; Thermo Fisher Scientific) (5.5 mmol/L D-glucose). Immortalized human keratinocytes (HaCaTs) were grown in low-glucose DMEM medium (NG) (5.5 mmol/L D-glucose) (Life Technologies, Gaithersburg, MD). The cells were maintained in a standard culture incubator with humidified air containing 5% CO₂ at 37°C. For induction of hyperglycemia, MCDB-131 or DMEM medium was added with additional 25 mmol/L D-glucose (HG). Cells cultured in L-glucose (LG) (25 mmol/L) and D-mannitol (mannitol) (20 mmol/L) were used as osmolality control (21).

ZEB1 siRNA Transfection

HMECs were seeded (0.1×10^6 cells) per well in a 12-well plate in antibiotic-free medium. Transfection was performed at 70% confluency using DharmaFECT reagent (GE Dharmacon) and OptiMEM (Thermo Fisher Scientific) using siRNA smart pool for human *ZEB1* (50 nmol/L) or control scrambled siRNA. mRNA analysis or functional assays were done with cells collected 72 h posttransfection.

LDL Uptake Assay

DyLight 550-labeled human LDL (10 μ g/mL) was added to HMECs transfected with either control or *ZEB1* followed by incubation at 37°C for 4 h. Cells were then washed with PBS. Acetylated LDL uptake was then analyzed by fluorescence microscopy, and quantification was done using ZEN 2 software.

In Vitro Angiogenesis Assay

Tube formation on Matrigel was assessed as a determinant of in vitro angiogenesis (22,23). Briefly, HMECs were transfected with control or *ZEB1* siRNA or overexpression plasmid. Following 3 days of transfection, seeding was done at seeding density of 5×10^4 cells/well in a Matrigel-coated fourwell plate. In vitro angiogenesis was assessed by calculating the tube length post-6 h of seeding using fluorescence microscopy (24).

Immunocytochemistry, Immunohistochemistry, and Confocal Microscopy

For immunocytochemistry, HMECs or HaCaT cells (3×10^4 cells/well) were seeded on cover slip. After treatment, cells were fixed using immunocytochemistry fixation buffer (cat. no. 550010; BD Biosciences). It was followed by blocking with 10% normal goat serum and then incubation overnight with primary antibody against E-cadherin (1:400), FSP-1 (1:200), VEGF (1:200), and VE-cadherin (1:250). Visualization of signal was performed using specific secondary fluorescence-tagged antibody (1:250 dilution) and counterstained using DAPI. Imaging was done using an inverted fluorescence/confocal

microscope (Olympus FV1000). Image analysis was performed as described previously (25). The quantification of images were done using ImageJ (National Institutes of Health). For immunohistochemistry, tissue sections were incubated with specific primary antibodies against E-cadherin (1:400), ZEB1 (1:100), CD31 (1:250), SMA (1:400), collagen IV (1:400), β -catenin (1:400), F4/80 (1:200) and keratin-14 (1:1,000). This was followed by addition of fluorescent secondary antibodies (1:250 dilution).

Angiogenesis Protein Array

Cell lysates obtained from wound edge tissue of Zeb1^{+/-} or wild-type mice were subjected to proteome profiler array (ARY015; R&D Systems) according to the manufacturer's instructions. Data presented as pixel density normalized to the reference spots. CD31 and vWF proteins were not present in the array and, hence, were validated through immunohistochemistry separately.

RNA Isolation and Quantitative Real-time PCR

RNA extraction was done from wound tissue samples or cultured cells using the miRVana kit (cat. no. AM1560; Ambion). cDNA preparation was done from mRNA using qScript SuperMix (cat. no. 101414; Quanta Biosciences). Quantitative real-time PCR was done using SYBR green-based chemistry and primers specific for selected genes (Supplementary Table 4). Gene expression was quantified using the $\Delta\Delta C_t$ relative quantization method using 18S, β -actin alone, or their average as a normalization control.

Laser Capture Microdissection

Laser capture microdissection (LCM) was performed as reported previously by our group (26). Endothelial cell or epithelial cell-rich regions under 10 \times lens were captured based on the fluorescence and hematoxylin staining, respectively, into 25 μ L cell direct buffer (Invitrogen).

Ultrasound Data Acquisition and Analysis

Ultrasound imaging for the calculation of wound area and blood flow rate was done using the Vevo 2100 system as previously described (27,28).

Human Samples

Wound biopsy samples were obtained from patients with chronic wounds who were clinically diagnosed with diabetes or who did not have diabetes. The Declaration of Helsinki protocols were followed. Patients provided written informed consent under an institutional review board (The Ohio State University). The patients with diabetes ($n = 5$: 1 male, 4 female, 4 Caucasian, 1 African American) had mean age of 48.6 ± 6.8 years (mean \pm SD) with mean wound area of 8.2 ± 3.8 cm² (mean \pm SEM). The group without diabetes ($n = 5$: 3 male, 2 female, 4 Caucasian, 1 African American) had mean age of 50.4 ± 7.3 years (mean \pm SD) with mean wound area of 45.4 ± 31.9 cm² (mean \pm SEM).

Animal Studies and Lentiviral Delivery

db/db (BKS.Cg-m^{+/+}Lepr^{db/J}) mice were purchased (stock no, 000642; The Jackson Laboratory, Bar Harbor, ME). Zeb1 heterozygous mice were a kind gift from Dr. Douglas Dean at University of Louisville, Louisville, KY. Zeb1^{+/+} and Zeb1^{+/-} mice (8–10 weeks) were injected with streptozotocin (STZ) in the intraperitoneal region (50 mg/kg; 5 days) or citrate buffer (vehicle control [sodium citrate, 0.05 mol/L, 4.5 pH]). Mice were fasted for 6 h at the time of STZ injection with free access to water (29). One week after STZ injection, blood samples were collected by tail venopuncture of the mice and used for the estimation of blood glucose levels. Blood glucose levels were assessed using Accu-Chek glucometer (Roche, Basel, Switzerland). Animals with fasting (6 h) blood glucose levels for two consecutive readings of >250 mg/dL (~ 14 mmol) were considered diabetic (30). Wounding was performed after 4 weeks of STZ injection. The actual values of blood glucose levels before wounding were 25.5 ± 3.5 mmol/L for Zeb1^{+/+} and 26.2 ± 2.0 mmol/L for Zeb1^{+/-} animals ($n = 5$, all males; P value = 1, Mann-Whitney U test). Animal studies were conducted in accordance with approved protocols by the Laboratory Animal Care and Use Committee (The Ohio State University and Indiana University). The animals were tagged and grouped randomly. Delivery of siRNA lentivirus (Lv) particles was achieved by intradermal injection. Animal fur on the area of interest was trimmed prior to the transfection. The siRNA smart for mouse *Zeb1* in lentiviral vector and scrambled siRNA control Lv particles were intradermally injected into the wound edge skin 2 days before wounding (d -2) at titer 1×10^6 cfu/mL (50 μ L). The same process of injection was repeated on wounding day (d0) and at day 3 postwounding (d3).

Wound Models

Excisional wounds (6 mm in diameter) were created on the dorsal skin of Zeb1 wild-type and Zeb1^{+/-} animals as previously described by our group (31). For *db/db* mice, four excisional wounds were generated using 8-mm diameter biopsy punch (32). Every wound was subjected to digital photography and perfusion analysis using PeriCam PSI HR laser speckle (PeriMed, Järfälla, Sweden) every alternate day till study completion. The analyses of wound area were done using ImageJ software. The animals were subjected to euthanasia at their respective time points, and the wound edges were stored in optimal cutting temperature compound (OCT) for further analyses. For wound-edge harvest, 1–1.5 mm of the tissue from the leading edge of the wounded skin was excised around the entire wound (33). Furthermore, when specific cell type was of interest, LCM was employed.

ChIP Assay

ChIP assay was performed to evaluate ZEB1 binding to E-cadherin promoter in NG (low glucose: 5.5 mmol/L) and HG (MCDB-131 media with additional 25 mmol/L D-glucose) conditions (SimpleChIP Plus Enzymatic

Chromatin IP Kit). Briefly, NG- or HG-exposed HMECs were fixed for 10 mins at room temperature (1% formaldehyde) followed by addition of glycine. The cells were processed for nuclei preparation and pelleted nuclei incubated with micrococcal nuclease (cat. no. 10011; Cell Signaling Technology) for generating chromatin samples of fragment sizes averaging 150–900 base pairs. It was then followed by the addition of EDTA (0.5 mol/L) to stop the enzymatic reaction. Samples were then sonicated and centrifuged for 10 min at 10,000 RPM (4°C). ZEB1 antibody, anti-histone H3 antibody, or control normal rabbit IgG was added and incubated overnight at 4°C with rotation. Protein G-agarose beads were used to pellet down the antibody-chromatin complexes. The DNA immunoprecipitated after this step was then eluted followed by purification. PCR using specific primers flanking the promoter region of E-cadherin gene was then performed (Supplementary Table 4). Results were examined as percentage of input.

Coimmunoprecipitation Mass Spectrometry

Immunoprecipitation was performed using Dynabeads Co-Immunoprecipitation Kit (cat. no. 14321D; Thermo Fisher Scientific) as per the manufacturer's instruction. The bead-bound protein complex was subjected to in-solution digestion in Last Wash Buffer (LWB) (Dynabeads Co-Immunoprecipitation Kit) for direct mass spectrometry analysis.

Western Blot

Cells or homogenized tissues were harvested using cell lysis buffer (cat. no. 9803; Cell Signaling Technology), sonicated on ice (three pulses for 3 s), and centrifuged (14,000g for 20 min at 4°C). The protein estimation in the clear lysates was done using bicinchoninic acid assay. Proteins (25–30 µg) were separated on 4–12% Bis-Tris Gel/MOPS running buffer (NuPAGE, cat. nos. NP0321BOX and NP0001) (45 min at 200 V) using the NuPAGE electrophoresis system (Invitrogen). Proteins were transferred to polyvinylidene difluoride membranes (2.15 h at 30 V). Membranes were blocked with 5% skim milk in Tris-buffered saline with 0.1% Tween 20 for 1 h at room temperature and incubated with the respective primary antibodies overnight at 4°C. The following day the membranes were washed and incubated with the corresponding horseradish peroxidase-conjugated secondary antibody for 1h at room temperature. The membranes were washed and the images were acquired using HyGLO chemiluminescent detection reagent (cat. no. E-2500; Thermo Scientific, Swedesboro, NJ) and Azure c600 Gel Imaging System by Azure Biosystems. β-Actin and α-tubulin were used as loading control. Image J (National Institutes of Health) software was used for quantification of bands by densitometry analysis. For Western blot, polyvinylidene difluoride membranes were incubated with specific primary antibodies against ZEB1 (cat. no. PA5-28221, 1:500; Invitrogen), FSP-1 (cat. no. ab27957, 1:500; Abcam), E-cadherin (cat. no. 13-1700, 1:2,000;

Invitrogen), β-actin (cat. no. 5441, 1:2,500; Sigma-Aldrich), and α-tubulin (cat. no. ab18251, 1:2,500; Abcam).

SILAC Labeling

Triple SILAC labeling of the HaCaT cells was done according to our previous report with slight modification (32). Cells were grown for six passages in L-arginine- and L-lysine-deficient SILAC DMEM media (cat. no. 88420; Thermo Fisher Scientific). Labeling was done using different light or heavy L-lysine or L-arginine at a concentration of 50 mg/L (all from Thermo Fisher Scientific) added with 10% FBS (dialyzed). For light media, L-lysine-2HCl (cat. no. 88429) and L-arginine-HCl (cat. no. 88427) were added. For heavy media, addition of L-lysine-2HCl, ¹³C₆, ¹⁵N₂ (cat. no. 88209), and L-arginine-HCl, ¹³C₆, ¹⁵N₄ (cat. no.89990), was done. For medium media, ¹³C₆ L-arginine (cat. no. 88210) and L-lysine-2HCl, 4,4,5,5-D4 (cat no. 88437), were added. The incorporation levels of medium and heavy isotopes were tested using mass spectrometry based on shift in the mass as compared with light isotope. After confirmation of >95% labeling, the experiments were performed. HaCaT cells were transfected with either 0.5 µg ZEB1 overexpression plasmid in cells grown in heavy media or 2 µg ZEB1 overexpression plasmid in cells grown in medium media. HaCaT cells transfected with control plasmid and cultured in light media were used for profiling basal protein levels. Differential protein ratios were calculated using unique peptide intensity between medium, heavy, and light isotope-labeled peptides using two-dimensional liquid chromatography-tandem mass spectrometry as described previously (34). Data were searched on Proteome Discoverer using SEQUEST against human UniProt database (Thermo Fisher Scientific) as per our previous report (34). Protein-protein interaction of significant proteins among the groups was searched using Search Tool for the Retrieval of INteracting Genes/proteins (STRING) (version 10.0) (<http://string-db.org/>) using a high-confidence cutoff (0.9). Additionally, Ingenuity pathway analysis (IPA) (Ingenuity Systems) was used to explore the biological functions affected due to ZEB1 overexpression or silencing during NG or HG conditions as described previously (35,36).

Statistical Analysis

Normality of distribution among data was assessed using the Kolmogorov-Smirnov test. Student *t* test (two-tailed) or ANOVA was used to test the significant differences among groups where data were found to be normally distributed (*P* value >0.05, Kolmogorov-Smirnov test). In case of ANOVA, Tukey honestly significant difference (HSD) post hoc test was applied. In the pairwise comparison where normality check was not possible, we have used Mann-Whitney *U* test or Kruskal-Wallis test. A *P* value of <0.05 was considered significant.

Data and Resource Availability

The data that support the findings of this study are available from the corresponding authors upon reasonable request.

RESULTS

E-Cadherin/ZEB1 Causes Injury-Induced Transient EMT

In mice, cutaneous wounding resulted in loss of epithelial marker *E-cadherin* with concomitant gain of mesenchymal markers β -catenin, collagen type I (*Col1a1*), and fibroblast-specific protein *FSP-1* (Fig. 1A–D). At the wound edge, such loss of *E-cadherin* was also associated with increased levels of its EMT-inducing transcriptional repressors, *Zeb1* and *Zeb2* (Fig. 1E and F and Supplementary Fig. 1A and B). In BL6 mice, this inverse expressional levels of *Zeb1* and *E-cadherin* was more prominent at day 5 postwounding. To understand the significance of ZEB1 signaling in transient wound EMT, we studied *Zeb1* heterozygous (*Zeb1*^{+/-}) mice, as *Zeb1*-null (*Zeb1*^{-/-}) mice are not viable (37). Cutaneous wound-edge tissue of *Zeb1*^{+/-} mice showed lower levels of *Zeb1* compared with their wild-type (*Zeb1*^{+/+}) littermates (Supplementary Fig. 1C). Increased levels of *E-cadherin* in day 7 wound-edge epithelium of *Zeb1*^{+/-} mice pointed toward the notion of a defective wound EMT process (Fig. 1G–J). In further support, wound edge of these *Zeb1*^{+/-} mice showed lower levels of vimentin (*Vim*), *FSP-1*, and β -catenin expression (Fig. 1K and L and Supplementary Fig. 1D–F). Taken together, these parameters established that EMT was defective in the wound edge of *Zeb1*^{+/-} mice. To test a direct cause-and-effect relationship between ZEB1 and wound-edge EMT, we conducted gene manipulations in vitro. siRNA-mediated depletion of *ZEB1* in human keratinocytes bolstered epithelial characteristics as manifested by elevated levels of *E-cadherin* (Supplementary Fig. 1G–J). Concurrent compromise in mesenchymal characteristics, as represented by lower *FSP-1*, was noted (Supplementary Fig. 1K and L). Additionally, SILAC proteomic analysis identified that graded overexpression of ZEB1 attenuated cell-cell adhesion, a known hallmark of EMT (Supplementary Fig. 2A–F). Elevated ZEB1 caused such wound-edge EMT by downregulating proteins involved in cytoskeletal, cell junction, and adherens junction networks (Supplementary Tables 1 and 2).

Low Wound Edge ZEB1 Compromised Injury-Induced Angiogenesis

ZEB1 knockdown caused dysfunction of HMECs as manifested by attenuated Matrigel tube formation as well as lower uptake of acetylated LDL (Supplementary Fig. 3A–D). Consistently, moderate *ZEB1* overexpression (~50- to 200-fold) enhanced angiogenic functions of HMECs (Supplementary Fig. 3E and F). However, extreme overexpression of *ZEB1* (~600-fold) displayed detrimental effects

including loss of endothelial function and cytotoxicity (Supplementary Fig. 3F–I). Such dichotomy in ZEB1 function, hitherto unknown, informed follow-up in vivo studies and related data interpretation. Under conditions of ZEB1 deficiency as in *Zeb1*^{+/-} mice, wound-edge angiogenic markers were lower compared with their wild-type littermates (Fig. 2A and B and Supplementary Fig. 3J). Such endothelial dysfunction in response to low ZEB1 was further characterized using an angiogenesis-related protein array. Of 53 angiogenesis-related proteins screened, the expression levels of 10 were downregulated in *Zeb1*^{+/-} animals compared with wild-type animals. Candidates lower in *Zeb1*^{+/-} mice were angiogenin, coagulation factor III, CD26, collagen XVIII, matrix metalloproteinase (MMP-3), MMP-9, osteopontin, CXCL12, serpin E1, and serpin F1 (Fig. 2C and D). In general, these proteins account for endothelial cell proliferation, migration, basement membrane invasion, and maintenance of vascular integrity in vivo. The ability of wound-edge CD31⁺ endothelial cells to make blood vessels was tested through colocalization with different functional markers, vWF and SMA (Fig. 2E–H). Lower prevalence of CD31⁺/vWF⁺ and CD31⁺/SMA⁺ vasculature was observed in wound-edge tissue of *Zeb1*^{+/-} mice compared with wild-type mice (Fig. 2F and H).

ZEB1 Deficiency Delayed Cutaneous Wound Closure and Angiogenesis

Zeb1^{+/-} mice were wounded, and their wound vascularization and reepithelization rates were compared with outcomes from corresponding wild-type mice. Wound tissue of *Zeb1*^{+/-} mice suffered from poor perfusion as assessed by a quantitative high-resolution laser speckle imaging system (Fig. 3A and B). At the wound site, arterial pulse pressure as measured using high-resolution color Doppler was also lower in *Zeb1*^{+/-} mice (Fig. 3C and D and Supplementary Video 1A). For addressing the potential role of residual ZEB1 in these heterozygous mice, lentiviral knockdown of ZEB1 was achieved at the wound site of *Zeb1*^{+/-} mice. Interestingly, such further lowering of ZEB1 at the wound site caused additional attenuation of wound tissue perfusion, adding credence to the notion that ZEB1 plays a major role in enabling vascularization of the cutaneous wound tissue (Supplementary Fig. 4A–D). However, we did observe some variability in wound perfusion outcome in the lentiviral intervention group on days 9 and 11 postwounding. Such variability is not uncommon in response to viral vector delivery (38). Wound closure was compromised in *Zeb1*^{+/-} mice (Fig. 3E). When the wounds of control wild-type mice approached full closure, wounds in mice deficient in ZEB1 remained roughly open by a third of its initial area (Fig. 3F–I and Supplementary Video 1B). Comparable impairment of healing was evident in independent studies on *Zeb1*^{+/+} and *Zeb1*^{+/-} mice subjected to Lv knockdown of wound site ZEB1 (Supplementary Fig. 4E–J).

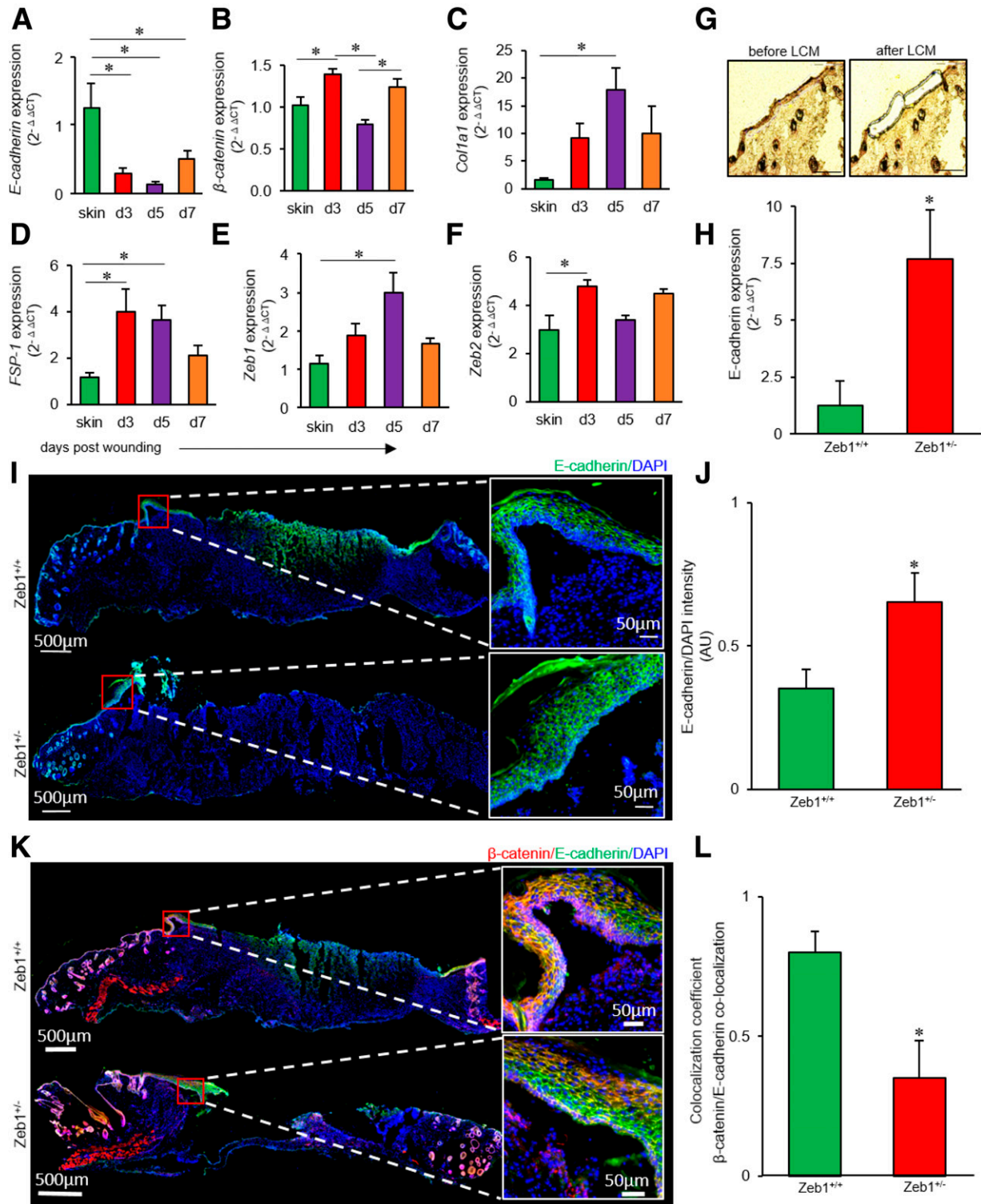


Figure 1—*E-cadherin*/ZEB1 causes injury-induced transient EMT. Quantitative RT-PCR analyses of *E-cadherin* (A), β -catenin (B), *Col1a1* (C), *FSP-1* (D), *Zeb1* (E), and *Zeb2* (F) expression in cutaneous wounds of BL6 mice at different time points postwounding. Data are represented as the mean \pm SEM ($n = 7-11$). $*P < 0.05$ (one-way ANOVA, followed by Tukey HSD post hoc test). G: Representative figure shows the selection of epithelial-rich tissue elements and their collection before and after the LCM. Scale bars, 150 μ m. H: Quantitative RT-PCR analysis of *E-cadherin* levels in LCM-captured epithelial elements from day 7 wounds of Zeb1^{+/-} mice and Zeb1^{+/+} mice ($n = 8, 6$). $*P < 0.001$ (Student *t* test). Data are represented as the mean \pm SD. Immunohistochemical analysis of *E-cadherin* (I) and the intensity calculation (J) in day 7 wound edge of Zeb1^{+/-} mice vs. Zeb1^{+/+} mice. $n = 6$. $*P < 0.05$ (Student *t* test). Immunohistochemical analysis for *E-cadherin*– β -catenin colocalization (K) and the colocalization calculation (L) in day 7 wound edge of Zeb1^{+/-} mice vs. Zeb1^{+/+} mice. $n = 6$. $*P < 0.05$ (Student *t* test). Data are represented as the mean \pm SEM. AU, arbitrary units.

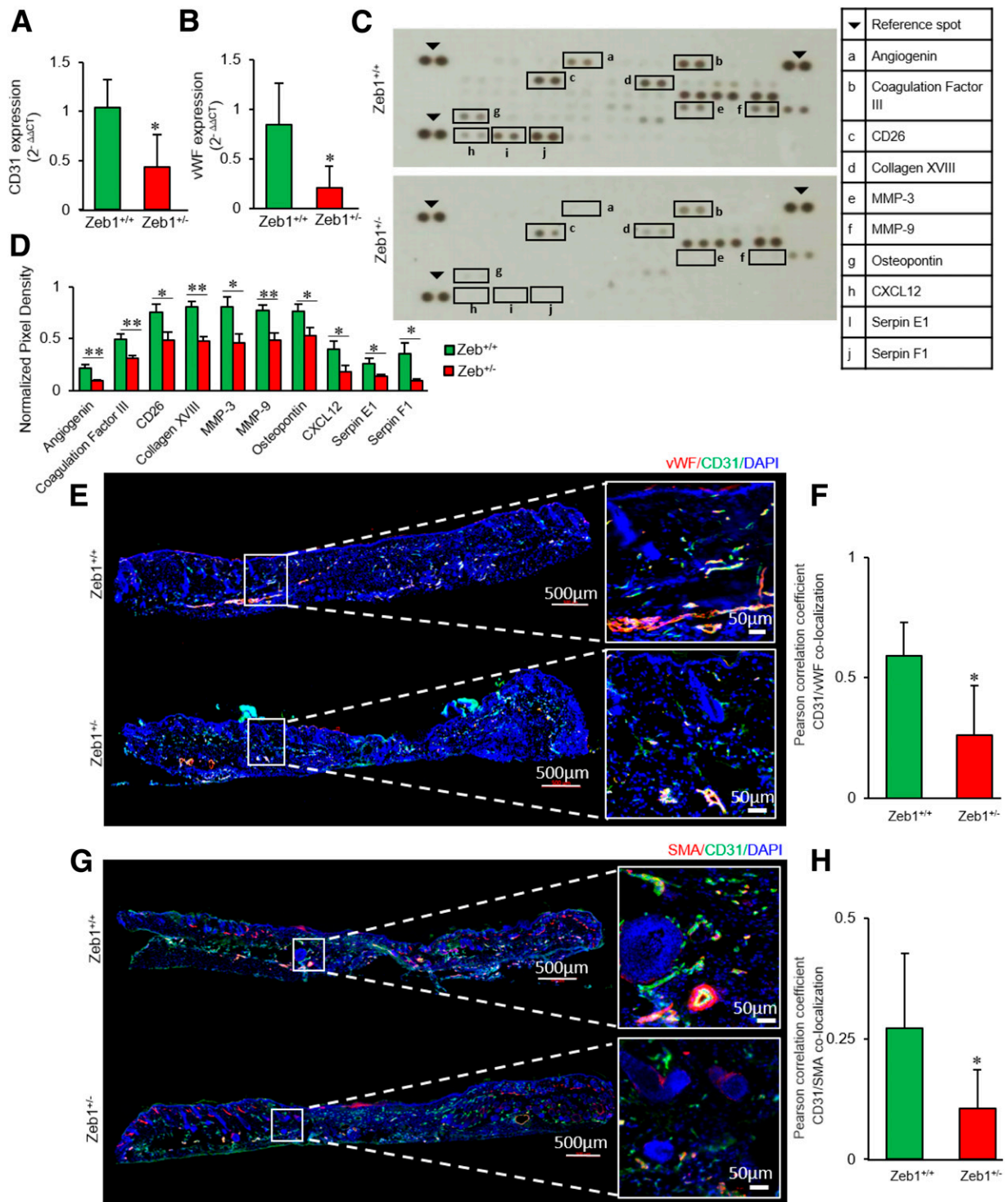


Figure 2—Low wound-edge ZEB1 compromised injury-induced angiogenesis. Quantitative RT-PCR analyses of CD31 (A) and vWF (B) in day 13 wound edge of Zeb1^{+/-} mice vs. Zeb1^{+/+} mice. *n* = 7. **P* < 0.05 (Student *t* test). Data are represented as the mean ± SD. C: Mouse angiogenesis array of day 13 wound edge proteins of Zeb1^{+/-} mice vs. Zeb1^{+/+} mice. D: Proteins that show obvious changes between the Zeb1^{+/-} mice and Zeb1^{+/+} mice are listed and quantified. *n* = 4, with two spots quantified for each protein. **P* < 0.05, ***P* < 0.01 (Student *t* test). Immunohistochemical analysis of CD31⁺/vWF⁺ coexpression (E) and their colocalization (F) in day 13 wound edge of Zeb1^{+/-} mice vs. Zeb1^{+/+} mice. *n* = 6. **P* < 0.05 (Student *t* test). Immunohistochemical analysis of CD31⁺/SMA⁺ coexpression (G) and their colocalization (H) in day 13 wound edge of Zeb1^{+/-} mice vs. Zeb1^{+/+} mice. *n* = 6. **P* < 0.05 (Student *t* test). Data are represented as the mean ± SD.

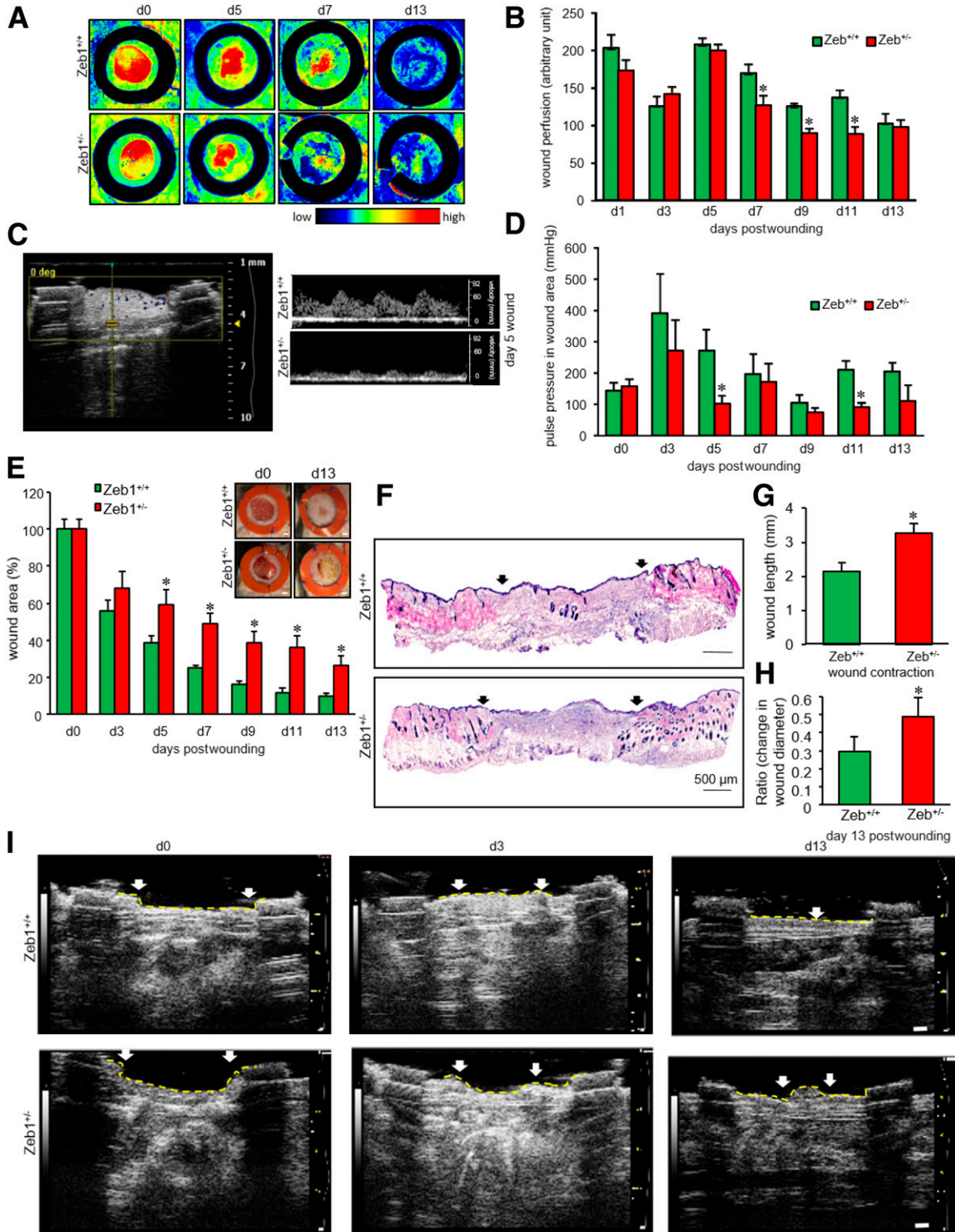


Figure 3—ZEB1 deficiency delayed cutaneous wound angiogenesis and closure. PeriMed laser speckle–assisted wound perfusion images (A) and analysis of wounds (B) of Zeb1^{+/-} mice vs. Zeb1^{+/+} mice ($n = 6, 8$ wounds). $*P < 0.05$ (Student t test). Wound edge blood flow (C) and pulse pressure (D) were measured using the color Doppler feature of Vevo 2100 ($n = 6$ wounds). $*P < 0.05$ (Student t test). E: Wound closure was monitored at different days postwounding in Zeb1^{+/-} mice vs. Zeb1^{+/+} mice by digital planimetry and was presented as percentage of wound area ($n = 6, 8$ wounds). $*P < 0.05$ (Student t test). F: Representative images of wound biopsy tissue sections (10 μ m) of Zeb1^{+/-} mice vs. Zeb1^{+/+} mice (day 13) stained using hematoxylin (blue) and eosin (red). Scale bars, 500 μ m. Black arrows represent the initial wound. G: Bar graph represents the wound contraction in Zeb1^{+/-} mice vs. Zeb1^{+/+} mice. $n = 9$. $*P < 0.05$ (Student t test). Data are represented as the mean \pm SEM. In vivo wound contraction (H) and imaging (I) using Vevo 2100 for monitoring wound contraction and reepithelialization in Zeb1^{+/+} mice (upper panels) vs. Zeb1^{+/-} mice (lower panels). Scale bars, 1 mm. White arrows represent the region between wounds that is not reepithelialized. The yellow lines in images outline the cavitation area visualized by this imaging.

Hyperglycemia Induces ZEB1 and Impairs Its Binding to E-Cadherin Promoter

Hyperglycemia is widely recognized as a major factor that contributes to impaired healing in those with diabetes (39). LCM endothelial tissue from wound edge of diabetic wound patients showed strikingly elevated *ZEB1* expression (Fig. 4A). Such massive *ZEB1* elevation could be reproduced by exposing HMECs to a hyperglycemic condition, leading to loss of endothelial function (Fig. 4B and Supplementary Fig. 5A and B). Additional studies aimed at understanding how hyperglycemia caused such potent induction of *ZEB1* revealed that under conditions of hyperglycemia *ZEB1* turnover is high (Supplementary Fig. 5C). *ZEB1* is known to repress E-cadherin expression. Efforts to understand the significance of elevated *ZEB1* under conditions of hyperglycemia led to the investigation of its corepressors such as COOH-terminal binding protein (CtBP), histone deacetylase 1 (HDAC1), and BRM/SWI2-related gene (BRG) (40–42). Interestingly, hyperglycemia-dependent induction was specific for *ZEB1*, while expression of the other corepressors remain unchanged (Supplementary Fig. 5D–I). Follow-up studies therefore focused on understanding the significance of hyperglycemia-induced *ZEB1* expression. ChIP assay demonstrated that the binding of *ZEB1* to E-cadherin promoter was compromised under hyperglycemic conditions (Fig. 4C). Inhibition of *ZEB1* rescued the tube formation ability in HMECs challenged with hyperglycemia (Fig. 4D and E).

To gain further mechanistic insights into the differential action of *ZEB1* under normoglycemic and hyperglycemic conditions, we performed immunoprecipitation–mass spectrometry (Fig. 4F and G). Here, the aim was to identify putative proteins that physically associated with *ZEB1* under normoglycemic or hyperglycemic conditions. This effort led to the identification of 41 *ZEB1*-interacting proteins (Supplementary Table 3 and Fig. 4G). Among them, α -enolase (ENO1), poly(U)-binding-splicing factor (PUF60), actin cytoplasmic 1, serine/arginine-rich splicing factor (SRSF)1, SRSF3, SRSF5, SRSF6, SRSF8, testis-specific protein kinase (TESK1), and RNA binding protein kinase (RBM39) are annotated as *ZEB1* interactors in the ENCODE database (43). Only 8 (ENO1, S100A8, S100A9, PUF60, serpin B4, Daple, trypsin-1, and tubulin- α) out of these 41 interactors associated with *ZEB1* under normoglycemic, but not hyperglycemic, conditions (Fig. 4G and Supplementary Fig. 5J and K). Only one such protein uniquely interacted with *ZEB1* under hyperglycemic conditions. This protein, diphosphoinositol pentakisphosphate kinase 2 (PPIP5K2), shares binding interaction with CtBP1, a cooperative corepressor of *ZEB1* (44). The remaining 32 proteins interacted with *Zeb1* agnostic of the glycaemic status.

To obtain a more global understanding of the significance of *ZEB1* in the context of EMT, we investigated the effects of hyperglycemia on the epithelial cell proteome using triple SILAC proteomics (Supplementary Fig. 5L and M). The experimental design had two conditions of *ZEB1*

induction: 1) moderate, as achieved by hyperglycemia in vitro; and 2) extreme, as observed in the wound tissue under in vivo conditions of diabetes and as can be reproduced by a combination of hyperglycemia and gene delivery in vitro. String analysis revealed that extreme overexpression of *ZEB1*-upregulated proteins related to apoptosis and negative regulation of cellular process gene ontology clusters (Supplementary Fig. 5N). Under hyperglycemic conditions, *ZEB1* knockdown rescued cell viability by upregulating survival pathways and attenuating cell death pathways. These findings recognize *ZEB1* as a hyperglycemia-inducible pathogenic mechanism. Of outstanding interest in this context is the observation that *ZEB1* knockdown under hyperglycemic conditions caused EMT (Fig. 4H–J).

ZEB1 Knockdown Rescued Diabetic Endothelial Dysfunction and Improved Wound Closure

In endothelial cells, basal *ZEB1* expression is low (Supplementary Fig. 6A and B). However, in response to induction of diabetes using low-dose STZ, endothelial *ZEB1* was potently induced (Supplementary Fig. 6C and D). The significance of *ZEB1* under condition of diabetes was studied by investigating *ZEB1*-deficient diabetic mice. In *Zeb1*^{+/-} mice, induction of endothelial *ZEB1* in response to diabetes was severely blunted (Supplementary Fig. 6C and D). Such condition led to marked rescue of vascular dysfunction and wound tissue perfusion (Fig. 5A and B). The wound-edge tissue of diabetic *Zeb1*^{+/-} mice displayed higher abundance of CD31⁺/vWF⁺ and CD31⁺/SMA⁺ blood vessels compared with those in diabetic mice where endothelial *ZEB1* was high (Fig. 5C and D and Supplementary Fig. 6E and F). Compared with such control diabetic mice, wound closure rate was significantly higher in diabetic *Zeb1*^{+/-} mice with low endothelial *ZEB1* (Fig. 5E–H and Supplementary Fig. 6G). These observations led to the notion that under conditions of diabetes, arrest of endothelial *ZEB1* has the potential to rescue vascular and wound closure complications. In addition, hyperglycemia also induced *Zeb1* in wound macrophages (Supplementary Fig. 6H and I). Thus, the significance of *ZEB1* knockdown was tested in another model of experimental diabetes, the *db/db* mice. Consistent with observations in the low-dose STZ diabetic mice, *ZEB1* levels in the skin of *db/db* mice were high (Fig. 6A). The magnitude of such difference was far more prominent in this latter *db/db* model, offering the opportunity to intervene and test the functional significance of *ZEB1* in wound vascular biology and closure. In vivo intradermal administration of *Zeb1* siRNA Lv to the wound edge of diabetic (*db/db*) mice reduced endothelial cell *ZEB1* (Fig. 6B and Supplementary Fig. 7A). Such successful depletion of *ZEB1* in *db/db* mice caused improvements in perfusion to the wound tissue (Fig. 6C and D). Higher blood flow at the wound site of *db/db* mice subjected to topical *ZEB1* knockdown was supported by histological studies demonstrating increased abundance of vasculature (Fig. 6E and F and Supplementary Fig. 7B and C).

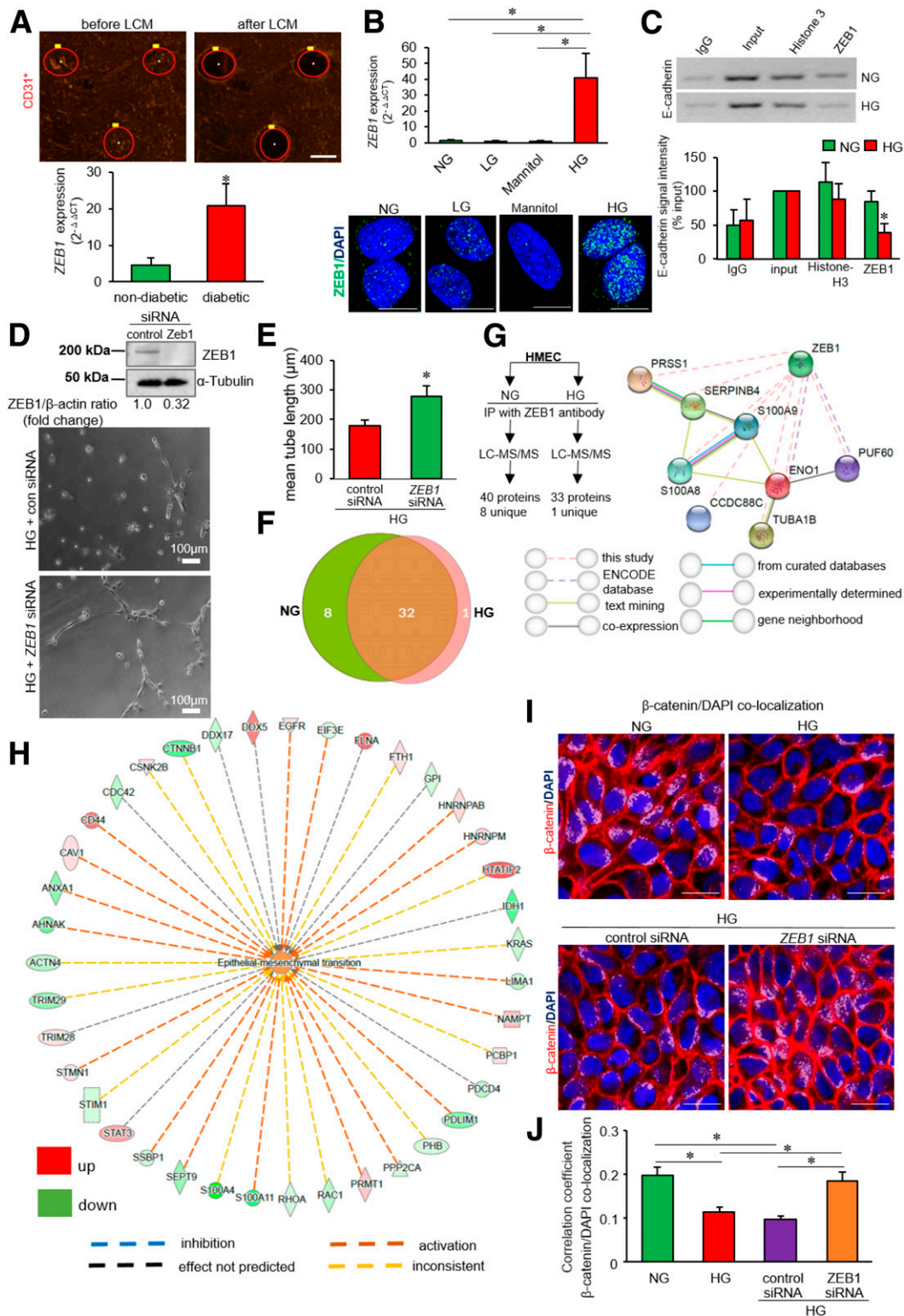


Figure 4—Hyperglycemia induces ZEB1 and impairs its binding to E-cadherin promoter. **A:** Top, representation of the selection of human CD31⁺ tissue elements (red) and their collection before and after the LCM. Scale bar, 150 μm. Bottom, quantitative RT-PCR analysis of ZEB1 levels in human diabetic and nondiabetic wounds. *n* = 5. **P* < 0.05 (Student *t* test). **B:** Top, quantitative RT-PCR analysis of ZEB1 expression in HMECs exposed to HG (25 mmol/L) or cultured in NG conditions. *n* = 6. **P* < 0.05 (Student *t* test). Cells cultured in LG (25 mmol/L) or mannitol (20 mmol/L) were used as osmolality control. Bottom, immunofluorescence analysis of ZEB1 in HMEC under NG/LG/mannitol/HG conditions. Scale bars, 10 μm. **C:** ChIP assay showing ZEB1 binding to E-cadherin promoter in NG- or HG-treated HMEC cells. IgG used as negative control, while histone H3 was used as positive control (*n* = 3). **P* < 0.05 (Kruskal-Wallis Test). ChIP signal was reported as percent of input at E-cadherin promoter. **D:** Top, Western blot analysis showing the knockdown of ZEB1 protein after cotreatment of ZEB1 siRNA in HG condition (*n* = 3). Bottom, Matrigel tube formation images and tube length (**E**) analysis in HMECs in HG condition and cotreatment with

Another relevant observation in this regard was that ZEB1 knockdown in otherwise ZEB1-rich *db/db* mice was associated with improved EMT. ZEB1 knockdown resulted in increased nuclear localization of β -catenin in the epithelial region (Supplementary Fig. 7D and E). Improved perfusion and elevated EMT following topical ZEB1 knockdown in *db/db* mice were associated with improved wound closure (Fig. 6G and H and Supplementary Fig. 7F–I).

DISCUSSION

EMT, a hallmark process of embryogenesis, is implicated in adult wound healing, fibrosis, and carcinogenesis (45,46). Several well-defined regulators including, but not limited to, extracellular factors (e.g., transforming growth factor- β , Notch ligands, fibroblast growth factor, and insulin-like growth factor), transcription factors (e.g., Twist and Zeb1), microRNAs (e.g., miR-200b, miR-200c, miR-9) and other microenvironmental cues (15,47) govern EMT. ZEB1, also known as TCF8 or DeltaEF1, is a member of the ZEB family of transcription factors, which is composed of two zinc-finger clusters (8). These zinc-finger clusters help ZEB1 bind to E-box DNA sequences. In addition to this, ZEB1 also contains binding domains including Smad interaction domain, CtBP interaction domain, and p300-P/CAF binding domain (8,48–50). By recruiting cosuppressors or coactivators using these domains, ZEB1 may either downregulate or upregulate gene expression (8,49). For example, ZEB1 represses E-cadherin expression by directly binding to the E-box located in the promoter and by recruiting the CtBP and/or BRG1, corepressors (42,51).

During cutaneous wound healing, under the influence of proinflammatory cytokines such as TNF- α , keratinocytes express mesenchyme-specific markers as exemplified by VIM and FSP-1 (3). Epithelial cells present adjacent to the wound bed are known to acquire mesenchymal markers in a bone morphogenetic proteins (BMP)-2/4-dependent manner (3). Such induction of EMT in wound-edge epithelial cells promotes wound reepithelialization. This work presents maiden evidence demonstrating a central role of ZEB1 in wound-edge EMT. Such process was greatly compromised, both in vitro and in vivo, following ZEB1 knockdown. The significance of ZEB1 in epithelial cells was therefore of interest. Unbiased interrogation using quantitative SILAC proteomics provided unprecedented insight into ZEB1-coregulated proteins that are likely to define the molecular underpinnings of wound EMT. Upregulation of ZEB1, as noted at the

wound-edge epithelium, in human keratinocytes caused downregulation of the largest subset of ZEB1-sensitive proteins. The primary clusters of these downregulated proteins included cytoskeletal, cell junction, and adherens junction proteins. Calreticulin, a Ca^{2+} -binding protein, was lowered following ZEB1 overexpression. Calreticulin controls cell-cell adhesion by regulating the expression of cytoskeletal vinculin (52). Indeed, transient downregulation of calreticulin weakens extracellular matrix attachment and facilitates EMT (53). It is known that low calreticulin-dependent EMT requires corepression of its interacting partners calnexin (CANX) and heat shock protein 90 (HSP90) (54). This work demonstrates that this entire cluster of EMT-regulating proteins was downregulated following ZEB1 overexpression, identifying ZEB1 as an upstream regulator of these molecular processes governing EMT. Other clusters of protein with known EMT-regulating properties that were identified as ZEB1 dependent include myosin protein classes (MYH4 and MYL1). These proteins are responsible for maintaining actin cytoskeleton organization (55). Thus, in the context of cutaneous wound healing, Zeb1 emerges as a hub regulator of multiple molecular pathways that govern EMT.

EMT and angiogenesis are two such wound healing related processes that are responsive to common upstream regulators (56,57). While in the epithelial cell compartment high ZEB1 enables EMT, in wound-related endothelial cells elevated ZEB1 not only is a key inducer of angiogenesis but also does so in a glycemic status-dependent manner. This work presents direct evidence establishing Zeb1 as a major regulator of wound angiogenesis. In the ZEB1 path of wound angiogenesis, VEGF signaling plays a central role. In ZEB1-deficient mice, proteins involved in VEGF signaling pathway were downregulated. During the wound healing process, coagulation factor III, derived from blood clot, drives the induction of VEGF and SMA necessary for neovascularization (58). ZEB1 deficiency compromised the level of coagulation factor III followed by blunted VEGF signaling. In addition, ZEB1 deficiency compromised the expression of MMP-9 known to act upstream of VEGF in the angiogenic pathway (59). Furthermore, angiogenin, a downstream effector molecule of VEGF signaling and a potent angiogenesis regulator, was also low in the wound edge of ZEB1^{+/-} mice. Taken together, multiple lines of evidence support that endothelial ZEB1 functions via the VEGF signaling path in driving wound angiogenesis.

control (con) siRNA or ZEB1 siRNA. Scale bar, 100 μm . $n = 6$. * $P < 0.05$ (Student t test). Data are represented as the mean \pm SD. F: Venn diagram of interacting partners of ZEB1 in NG and HG conditions obtained through immunoprecipitation mass spectrometric analysis in HMECs. A total of 41 proteins were identified to be interacting with ZEB1 during these conditions. G: Protein-protein interaction network of 8 proteins interacting with ZEB1 during NG but not in HG conditions using STRING, version 10.5. IP, immunoprecipitation. H: IPA of the proteins differentially expressed after ZEB1 silencing in HG condition (HaCaT) indicates the increase in EMT process. I and J: Immunofluorescence staining of β -catenin (red) and its nuclear colocalization (white) (I) and the correlation coefficient of β -catenin-DAPI colocalization in HaCaT cells (J) after treatment with control siRNA or ZEB1 siRNA under NG/HG conditions. Scale bars, 20 μm . $n = 5$ –7. * $P < 0.05$ (one-way ANOVA, followed by Tukey HSD post hoc test). Data are represented as the mean \pm SEM. LC-MS/MS, liquid chromatography-tandem mass spectrometry.

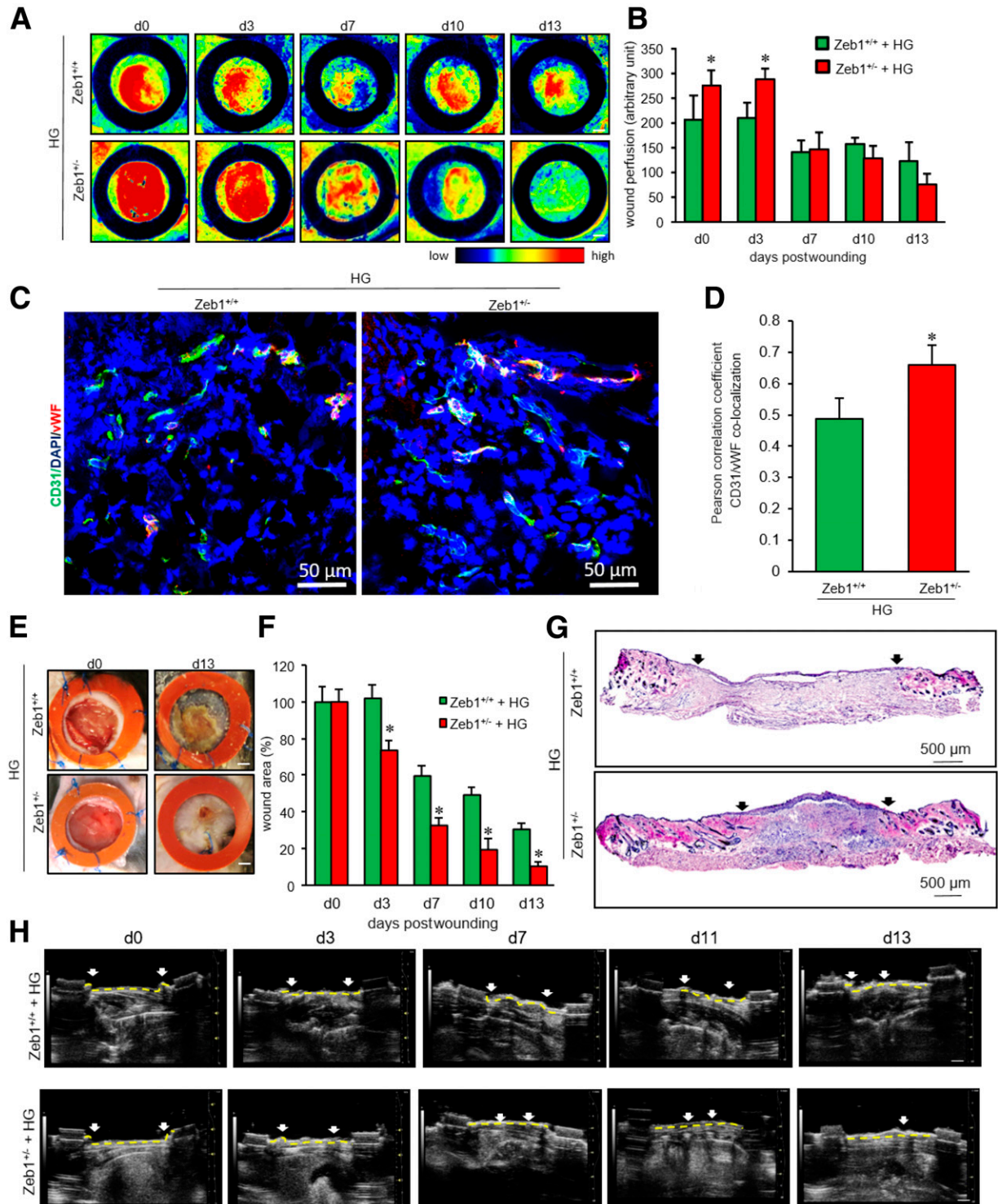


Figure 5—ZEB1 knockdown rescued diabetic endothelial dysfunction and improved wound closure. Zeb1^{+/-} mice and Zeb1^{+/+} mice were made diabetic through injection with STZ in the intraperitoneal region (50 mg/kg for 5 days). Diabetic mice were wounded, and wound perfusion and closure were monitored. Laser speckle imaging wound perfusion images (A) and their analyses (B) of wounds of STZ-treated diabetic Zeb1^{+/-} mice vs. Zeb1^{+/+} mice. *n* = 6 wounds. **P* < 0.05 (Student *t* test). Immunohistochemical analysis of CD31⁺/WF⁺ coexpression in wound edge of STZ-treated diabetic Zeb1^{+/-} mice vs. Zeb1^{+/+} mice (C) and its colocalization analysis (D). *n* = 6, **P* < 0.05 (Student *t* test). E: Wound closure was monitored at different days postwounding in STZ-treated diabetic Zeb1^{+/-} mice vs. Zeb1^{+/+} mice by digital planimetry. F: Data were presented as percentage of wound area. *n* = 6 wounds. **P* < 0.05 (Student *t* test). G: Representative images of wound biopsy tissue sections (10 μm) of STZ-treated diabetic Zeb1^{+/-} mice vs. Zeb1^{+/+} mice (day 13) stained using hematoxylin (blue) and eosin (red). Scale bars, 500 μm. H: In vivo wound imaging using Vevo 2100 for monitoring wound contraction and reepithelialization in STZ-treated diabetic Zeb1^{+/+} mice (upper panels) vs. Zeb1^{+/-} mice (lower panels). Scale bars, 1 mm. White arrows represent the region between wounds that is not reepithelialized. The yellow lines in images outline the cavitation area visualized by this imaging. Data are represented as the mean ± SD.

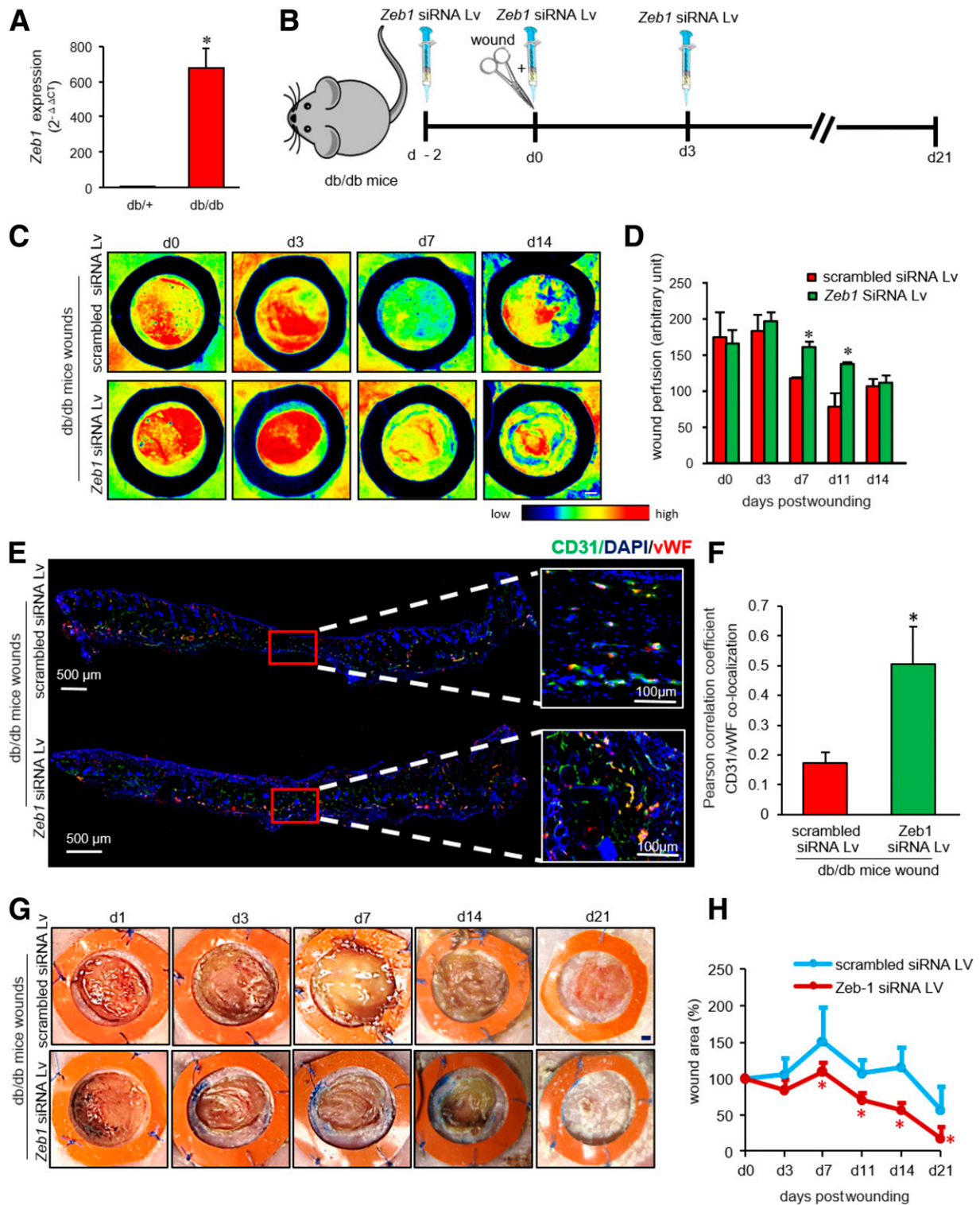


Figure 6—ZEB1 knockdown in *db/db* mice rescued endothelial dysfunction and improved wound closure. **A**: Quantitative RT-PCR analysis of *Zeb1* expression in skin of *db/db* diabetic mice vs. *db/+* control littermates. *n* = 4. **P* < 0.05 (Student *t* test). **B**: Schematic diagram showing intradermal delivery of *Zeb1* siRNA Lv or scrambled siRNA Lv to the dorsal skin of *db/db* mice. PeriMed laser speckle-assisted wound perfusion images (**C**) and their analysis (**D**) of wounds of *db/db* mice injected with *Zeb1* siRNA Lv or scrambled siRNA Lv. *n* = 4 wounds. **P* < 0.05 (Student *t* test). Immunohistochemical analysis of CD31⁺/vWF⁺ coexpression in wound edge of *db/db* mice injected with *Zeb1* siRNA Lv or scrambled siRNA Lv at day 21 postwounding (**E**) and its colocalization coefficient (**F**). *n* = 5 wounds. **P* < 0.05 (Student *t* test). **G**: Wound closure was monitored at different days postwounding in wounds of *db/db* mice injected with *Zeb1* siRNA Lv or scrambled siRNA Lv by digital planimetry. **H**: Data were presented as percentage of wound area. *n* = 8 wounds. **P* < 0.05 (Student *t* test). Data are represented as the mean ± SD.

Persistent hyperglycemia, as noted in diabetes, is widely known to stall wound healing. In trying to understand the significance of glycemic status in wound angiogenesis, this work led to a striking observation that led to the notion that both insufficient ZEB1 and excessive ZEB1 oppose wound angiogenesis. Efforts to test the hypothesis that hyperglycemia depletes ZEB1 and therefore dampens wound angiogenesis resulted in the unexpected finding that persistent hyperglycemia potently induced ZEB1. Of relevance, such extreme induction of ZEB1 has been reported for cells related to tumor angiogenesis (17). In this work, CHIP studies conducted under conditions of hyperglycemia provided insight into the mechanistic bases of ZEB1 interaction with E-cadherin. Hyperglycemia diminished the physical association of ZEB1 with E-cadherin promoter, thereby releasing E-cadherin from ZEB1-dependent repression. Loss of control over E-cadherin repression is known to cause microvascular endothelial dysfunction commonly observed in people with diabetes (60). Restrained expression of E-cadherin is noted in the intima of human aorta. Such restraint is lost under disease conditions such as atherosclerosis (61). In this work, the study of proteins that interact with ZEB1 identified that ENO-1 bound to ZEB1 is released under conditions of hyperglycemia. The reported presence of conserved canonical E-boxes in ENO-1 may explain ZEB1-ENO1 binding (62). Under conditions of hyperglycemia, the binding of Sp1 to E-box is markedly induced (63,64). Considering that the binding of E-box of ZEB1 is competitive with that of Sp1, it is plausible that under hyperglycemia, excessive Sp1 binding competitively inhibits ZEB1 binding. Free ENO-1, unbound to ZEB1, poses an inflammatory threat in the context of hyperglycemia (65). This work reports that proinflammatory S100A8/A9 also binds to ZEB1. Such binding is impaired under hyperglycemia, resulting in higher levels of free serum S100A8/A9 in patients with diabetes (66). In the context of our findings, it is important to note that in vascular smooth muscle cells diabetes causes loss of Zeb1 occupancy at the MCP-1 and COX-2 promoter (67). Such loss enhances binding of monocytes to diabetic vascular smooth muscle cells. It is plausible that alterations in cellular Zeb1 levels influence the expression and function of inflammatory cytokines.

Taken together, this work recognizes ZEB1 as a significant mechanistic hub across epithelial and endothelial cells on the wound tissue microenvironment. In both of these cellular compartments, ZEB1 is responsive to the glycemic status of the injury microenvironment. Both low and excessive ZEB1 levels are pathogenic, pointing toward the critical need to tune ZEB1 levels to intermediary levels optimal for wound repair. In epithelial cells, ZEB1 induces EMT toward wound reepithelialization. This process is impaired under conditions of hyperglycemia. In endothelial cells, ZEB1 is directly implicated in hyperglycemia-induced dysfunction. Excessive ZEB1, under diabetic conditions, may also contribute to the commonly noted persistent inflammatory response. Studies on intervention

demonstrate that ZEB1-directed therapeutic strategies are productive in the rescue of wound-related diabetes complications.

Funding. This work was supported by National Institute of General Medical Sciences, National Institutes of Health, grant GM108014 and also, in part, grant GM077185. This work was also supported in part by National Institute of Diabetes and Digestive and Kidney Diseases grant DK076566.

Duality of Interest. Research programs lead by C.K.S. as well as by S.R. were supported by the Lilly Endowment INCITE (Indiana Collaborative Initiative for Talent Enrichment) program. No other potential conflicts of interest relevant to this article were reported.

Author Contributions. K.S. and C.K.S. conceived and designed the work. K.S., M.S., D.P., S.T., S.C.G., D.K., S.S., S.K.M., F.S.-G., and S.K. collected and analyzed data for this work and participated in the preparation of the manuscript. K.S., S.R., and C.K.S. wrote the manuscript. C.K.S. is the guarantor of this work and, as such, had full access to all the data in the study and takes responsibility for the integrity of the data and the accuracy of the data analysis.

References

- Okonkwo UA, DiPietro LA. Diabetes and wound angiogenesis. *Int J Mol Sci* 2017;18:1419
- Okano J, Kojima H, Katagi M, et al. Hyperglycemia induces skin barrier dysfunctions with impairment of epidermal integrity in non-wounded skin of type 1 diabetic mice. *PLoS One* 2016;11:e0166215
- Yan C, Grimm WA, Garner WL, et al. Epithelial to mesenchymal transition in human skin wound healing is induced by tumor necrosis factor- α through bone morphogenetic protein-2. *Am J Pathol* 2010;176:2247–2258
- Tonnesen MG, Feng X, Clark RA. Angiogenesis in wound healing. *J Invest Dermatol Symp Proc* 2000;5:40–46
- Sen CK. Wound healing essentials: let there be oxygen. *Wound Repair Regen* 2009;17:1–18
- Chiu LY, Hsin IL, Yang TY, et al. The ERK-ZEB1 pathway mediates epithelial-mesenchymal transition in pemetrexed resistant lung cancer cells with suppression by vinca alkaloids. *Oncogene* 2017;36:242–253
- Sánchez-Tilló E, Siles L, de Barrios O, et al. Expanding roles of ZEB factors in tumorigenesis and tumor progression. *Am J Cancer Res* 2011;1:897–912
- Zhang P, Sun Y, Ma L. ZEB1: at the crossroads of epithelial-mesenchymal transition, metastasis and therapy resistance. *Cell Cycle* 2015;14:481–487
- Yi Y, Xie H, Xiao X, et al. Ultraviolet A irradiation induces senescence in human dermal fibroblasts by down-regulating DNMT1 via ZEB1. *Aging (Albany NY)* 2018;10:212–228
- Konradi S, Yasmin N, Haslwanter D, et al. Langerhans cell maturation is accompanied by induction of N-cadherin and the transcriptional regulators of epithelial-mesenchymal transition ZEB1/2. *Eur J Immunol* 2014;44:553–560
- Denecker G, Vandamme N, Akay O, et al. Identification of a ZEB2-MITF-ZEB1 transcriptional network that controls melanogenesis and melanoma progression. *Cell Death Differ* 2014;21:1250–1261
- Vincent-Mistiaen Z, Elbediwy A, Vanyai H, et al. YAP drives cutaneous squamous cell carcinoma formation and progression. *eLife* 2018;7:e33304
- Siles L, Ninfali C, Cortés M, Darling DS, Postigo A. ZEB1 protects skeletal muscle from damage and is required for its regeneration. *Nat Commun* 2019;10:1364
- Liu Y, El-Naggar S, Darling DS, Higashi Y, Dean DC. Zeb1 links epithelial-mesenchymal transition and cellular senescence. *Development* 2008;135:579–588
- Lamouille S, Xu J, Derynck R. Molecular mechanisms of epithelial-mesenchymal transition. *Nat Rev Mol Cell Biol* 2014;15:178–196
- Haensel D, Sun P, MacLean AL, et al. An Ovol2-Zeb1 transcriptional circuit regulates epithelial directional migration and proliferation. *EMBO Rep* 2019;20:e46273

17. Liu L, Tong Q, Liu S, et al. ZEB1 upregulates VEGF expression and stimulates angiogenesis in breast cancer. *PLoS One* 2016;11:e0148774
18. Magenta A, Cencioni C, Fasanaro P, et al. miR-200c is upregulated by oxidative stress and induces endothelial cell apoptosis and senescence via ZEB1 inhibition. *Cell Death Differ* 2011;18:1628–1639
19. Stone RC, Pastar I, Ojeh N, et al. Epithelial-mesenchymal transition in tissue repair and fibrosis. *Cell Tissue Res* 2016;365:495–506
20. Arumugam T, Ramachandran V, Fournier KF, et al. Epithelial to mesenchymal transition contributes to drug resistance in pancreatic cancer. *Cancer Res* 2009;69:5820–5828
21. El-Remessy AB, Abou-Mohamed G, Caldwell RW, Caldwell RB. High glucose-induced tyrosine nitration in endothelial cells: role of eNOS uncoupling and aldose reductase activation. *Invest Ophthalmol Vis Sci* 2003;44:3135–3143
22. Chan YC, Khanna S, Roy S, Sen CK. miR-200b targets Ets-1 and is down-regulated by hypoxia to induce angiogenic response of endothelial cells. *J Biol Chem* 2011;286:2047–2056
23. Chan YC, Roy S, Khanna S, Sen CK. Downregulation of endothelial microRNA-200b supports cutaneous wound angiogenesis by desilencing GATA binding protein 2 and vascular endothelial growth factor receptor 2. *Arterioscler Thromb Vasc Biol* 2012;32:1372–1382
24. Banerjee J, Das Ghatak P, Roy S, et al. Improvement of human keratinocyte migration by a redox active bioelectric dressing. *PLoS One* 2014;9:e89239
25. Das A, Ghatak S, Sinha M, et al. Correction of MFG-E8 resolves inflammation and promotes cutaneous wound healing in diabetes. *J Immunol* 2016;196:5089–5100
26. Roy S, Patel D, Khanna S, et al. Transcriptome-wide analysis of blood vessels laser captured from human skin and chronic wound-edge tissue. *Proc Natl Acad Sci U S A* 2007;104:14472–14477
27. Gallego-Perez D, Pal D, Ghatak S, et al. Topical tissue nano-transfection mediates non-viral stroma reprogramming and rescue. *Nat Nanotechnol* 2017;12:974–979
28. Gnyawali SC, Barki KG, Mathew-Steiner SS, et al. High-resolution harmonics ultrasound imaging for non-invasive characterization of wound healing in a pre-clinical swine model. *PLoS One* 2015;10:e0122327
29. Chaudhry ZZ, Morris DL, Moss DR, et al. Streptozotocin is equally diabetogenic whether administered to fed or fasted mice. *Lab Anim* 2013;47:257–265
30. Moriyama H, Wen L, Abiru N, et al. Induction and acceleration of insulinitis/diabetes in mice with a viral mimic (polyinosinic-polycytidylic acid) and an insulin self-peptide. *Proc Natl Acad Sci U S A* 2002;99:5539–5544
31. Ghatak S, Chan YC, Khanna S, et al. Barrier function of the repaired skin is disrupted following arrest of dicer in keratinocytes. *Mol Ther* 2015;23:1201–1210
32. Singh K, Pal D, Sinha M, et al. Epigenetic modification of microRNA-200b contributes to diabetic vasculopathy. *Mol Ther* 2017;25:2689–2704
33. Roy S, Khanna S, Nallu K, Hunt TK, Sen CK. Dermal wound healing is subject to redox control. *Mol Ther* 2006;13:211–220
34. Sinha M, Sen CK, Singh K, et al. Direct conversion of injury-site myeloid cells to fibroblast-like cells of granulation tissue. *Nat Commun* 2018;9:936
35. Das A, S El Masry M, Gnyawali SC, et al. Skin transcriptome of middle-aged women supplemented with natural herbo-mineral shilajit shows induction of microvascular and extracellular matrix mechanisms. *J Am Coll Nutr* 2019;38:526–536
36. Singh V, Jaiswal D, Singh K, et al. Azoospermic infertility is associated with altered expression of DNA repair genes. *DNA Repair (Amst)* 2019;75:39–47
37. Liu Y, Lu X, Huang L, et al. Different thresholds of ZEB1 are required for Ras-mediated tumour initiation and metastasis. *Nat Commun* 2014;5:5660
38. Feng Y, Nie L, Thakur MD, et al. A multifunctional lentiviral-based gene knockdown with concurrent rescue that controls for off-target effects of RNAi. *Genomics Proteomics Bioinformatics* 2010;8:238–245
39. Brem H, Tomic-Canic M. Cellular and molecular basis of wound healing in diabetes. *J Clin Invest* 2007;117:1219–1222
40. Postigo AA, Dean DC. ZEB represses transcription through interaction with the corepressor CtBP. *Proc Natl Acad Sci U S A* 1999;96:6683–6688
41. Wang J, Lee S, Teh CE, Bunting K, Ma L, Shannon MF. The transcription repressor, ZEB1, cooperates with CtBP2 and HDAC1 to suppress IL-2 gene activation in T cells. *Int Immunol* 2009;21:227–235
42. Sánchez-Tilló E, Lázaro A, Torrent R, et al. ZEB1 represses E-cadherin and induces an EMT by recruiting the SWI/SNF chromatin-remodeling protein BRG1. *Oncogene* 2010;29:3490–3500
43. Maher B. ENCODE: the human encyclopaedia. *Nature* 2012;489:46–48
44. Rouillard AD, Gundersen GW, Fernandez NF, et al. The harmonizome: a collection of processed datasets gathered to serve and mine knowledge about genes and proteins. *Database (Oxford)* 2016;2016
45. Hay ED. An overview of epithelio-mesenchymal transformation. *Acta Anat (Basel)* 1995;154:8–20
46. Kalluri R, Weinberg RA. The basics of epithelial-mesenchymal transition. *J Clin Invest* 2009;119:1420–1428
47. De Craene B, Bex G. Regulatory networks defining EMT during cancer initiation and progression. *Nat Rev Cancer* 2013;13:97–110
48. Postigo AA. Opposing functions of ZEB proteins in the regulation of the TGFbeta/BMP signaling pathway. *EMBO J* 2003;22:2443–2452
49. Postigo AA, Depp JL, Taylor JJ, Kroll KL. Regulation of Smad signaling through a differential recruitment of coactivators and corepressors by ZEB proteins. *EMBO J* 2003;22:2453–2462
50. Wellner U, Brabletz T, Keck T. ZEB1 in pancreatic cancer. *Cancers (Basel)* 2010;2:1617–1628
51. Wong TS, Gao W, Chan JY. Transcription regulation of E-cadherin by zinc finger E-box binding homeobox proteins in solid tumors. *BioMed Res Int* 2014;2014:921564
52. Opas M, Szewczenko-Pawlikowski M, Jass GK, Mesaali N, Michalak M. Calreticulin modulates cell adhesiveness via regulation of vinculin expression. *J Cell Biol* 1996;135:1913–1923
53. Leung-Hageteijn CY, Milankov K, Michalak M, Wilkins J, Dedhar S. Cell attachment to extracellular matrix substrates is inhibited upon downregulation of expression of calreticulin, an intracellular integrin alpha-subunit-binding protein. *J Cell Sci* 1994;107:589–600
54. Buck TM, Wright CM, Brodsky JL. The activities and function of molecular chaperones in the endoplasmic reticulum. *Semin Cell Dev Biol* 2007;18:751–761
55. Peckham M. How myosin organization of the actin cytoskeleton contributes to the cancer phenotype. *Biochem Soc Trans* 2016;44:1026–1034
56. Desai S, Laskar S, Pandey BN. Autocrine IL-8 and VEGF mediate epithelial-mesenchymal transition and invasiveness via p38/JNK-ATF-2 signalling in A549 lung cancer cells. *Cell Signal* 2013;25:1780–1791
57. Gonzalez-Moreno O, Lecanda J, Green JE, et al. VEGF elicits epithelial-mesenchymal transition (EMT) in prostate intraepithelial neoplasia (PIN)-like cells via an autocrine loop. *Exp Cell Res* 2010;316:554–567
58. Chen J, Kasper M, Heck T, et al. Tissue factor as a link between wounding and tissue repair. *Diabetes* 2005;54:2143–2154
59. Bergers G, Brekken R, McMahon G, et al. Matrix metalloproteinase-9 triggers the angiogenic switch during carcinogenesis. *Nat Cell Biol* 2000;2:737–744
60. Pankow JS, Decker PA, Berardi C, et al. Circulating cellular adhesion molecules and risk of diabetes: the Multi-Ethnic Study of Atherosclerosis (MESA). *Diabet Med* 2016;33:985–991
61. Bobryshev YV, Lord RS, Watanabe T, Ikezawa T. The cell adhesion molecule E-cadherin is widely expressed in human atherosclerotic lesions. *Cardiovasc Res* 1998;40:191–205
62. Kim JW, Zeller KI, Wang Y, et al. Evaluation of myc E-box phylogenetic footprints in glycolytic genes by chromatin immunoprecipitation assays. *Mol Cell Biol* 2004;24:5923–5936

63. Kolesnikoff N, Attema JL, Roslan S, et al. Specificity protein 1 (Sp1) maintains basal epithelial expression of the miR-200 family: implications for epithelial-mesenchymal transition. *J Biol Chem* 2014;289:11194–11205
64. Wutthisathapornchai A, Vongpipatana T, Muangsawat S, Boonsaen T, MacDonald MJ, Jitrapakdee S. Multiple E-boxes in the distal promoter of the rat pyruvate carboxylase gene function as a glucose-responsive element. *PLoS One* 2014;9:e102730
65. Choi J, Kim H, Kim Y, et al. The anti-inflammatory effect of GV1001 mediated by the downregulation of ENO1-induced pro-inflammatory cytokine production. *Immune Netw* 2015;15:291–303
66. Wang S, Song R, Wang Z, Jing Z, Wang S, Ma J. S100A8/A9 in inflammation. *Front Immunol* 2018;9:1298
67. Reddy MA, Jin W, Villeneuve L, et al. Pro-inflammatory role of microrna-200 in vascular smooth muscle cells from diabetic mice. *Arterioscler Thromb Vasc Biol* 2012;32:721–729